Nano Research Energy

ISSN 2791-0091 (print); 2790-8119 (online)
https://doi.org/10.26599/NRE.2025.9120153

Review Article

Transparent and flexible MXenes for supercapacitors and beyond

Iftikhar Hussain[1] (✉), Faiza Bibi[2], Muhammad Kashif Aslam[3], Xi Chen[1], Kejuan Meng[1], Momang Tian[1], Muhammad Zubair Khan[4], Muhammad Bilal Hanif[5], Debananda Mohapatra[6] (✉), and Kaili Zhang[1] (✉)

[1] *Department of Mechanical Engineering, City University of Hong Kong, Hong Kong 999077, China*
[2] *Sunway Centre for Electrochemical Energy and Sustainable Technology (SCEEST), School of Engineering and Technology, Sunway University, No. 5, Jalan Universiti, Bandar Sunway, 47500 Selangor Darul Ehsan, Malaysia*
[3] *Department of Chemical and Petroleum Engineering, College of Engineering, United Arab Emirates University, Al Ain 15551, Abu Dhabi, United Arab Emirates*
[4] *Department of Materials Science and Engineering, Pak-Austria Fachhochschule: Institute of Applied Sciences and Technology, Mang, Haripur, Khyber Pakhtunkhwa 22621, Pakistan*
[5] *Department of Inorganic Chemistry, Faculty of Natural Sciences, Comenius University Bratislava, 84215 Bratislava, Slovakia*
[6] *Graduate School of Semiconductor Materials and Devices Engineering, Ulsan National Institute of Science and Technology, 50 UNIST-gil, Ulju-gun, Ulsan 44919, Republic of Korea*

Received: 2 December 2024 / **Revised:** 9 January 2025 / **Accepted:** 10 January 2025 / **Published date:** 13 February 2025

ABSTRACT

MXenes are fast-growing two-dimensional (2D) carbides, nitrides, and carbonitrides nanomaterials exhibiting combined special features of high electronic conductivity, optoelectronic properties, and electrochemical properties with hydrophilicity character. The plasmonic characteristics of MXenes with optical nonlinearities associated with ultrafast dynamics empower it as one of the strongest candidates for transparent optoelectronic applications in the field of energy storage, conversion, photodetectors, quantum dot light-emitting diodes, smart windows, environmentally. It is timely to introduce and summarize a review article dedicated to the transparent MXene-based multifunctional applications that provide well-designed future roadmaps for these significant MXene smart materials. This review comprehensively discusses the transparent MXenes towards transparent electrodes for supercapacitors and beyond. The importance of MXene optoelectronic properties and tunability via composite materials incorporated with different polymers, oxides, sulfides, and carbonaceous nanomaterials are also thoroughly reviewed.

KEYWORDS

two-dimensional (2D) materials, MXene, transparent MXenes, energy storage, other applications

1 Introduction

Unlike a vast array of two-dimensional (2D) materials that encounter substantial hurdles regarding their synthesis and associated financial implications, MXenes have arisen as a distinctive class of emerging 2D nanomaterials with established and reliable soft chemical synthesis procedures, incorporating methods that utilize hydrofluoric acid (HF) as well as several modified acid techniques that have been developed progressively [1–4]. 2D MXenes offer versatile photonic, optoelectronic, and transparent electromagnetic shielding applications credited to their tunable optoelectronic properties compared to other 2D materials [1, 5]. The discovery of 2D $Ti_3C_2T_x$ in 2011 opened up many avenues in the field of 2D nanomaterials, leading to the exploration of a large family of transition metal carbides, nitride, and carbonitrides following the general formula $M_{n+1}X_nT_x$ [5], where M can be transition metals, X can be carbon, nitrogen, or both, and T_x reflects surface termination groups such as, –H, –OH, –F, etc. [6, 7]. These materials are exciting due to their remarkable electrical conductivity [1, 8], and the inherent hydrophilicity of these materials positions them as highly promising candidates for temperature sensor applications [9], pressure sensors [10], energy storage-conversion [11, 12], electromagnetic interference shielding, water remediation, optoelectronics, etc. [1, 13]. The metallic conductivity arises from the free electrons of either transition metal carbide or nitride core backbone, whereas the hydrophilicity originated from the wet chemical synthesis process. The combination of large lateral dimensions alongside their minimal atomic thickness results in an extensive surface area that is readily available for surface reactions, enhancing their utility in chemical and optoelectronic

Address correspondence to Iftikhar Hussain, ihussaintoori1@gmail.com; Debananda Mohapatra, debanandam@unist.ac.kr; Kaili Zhang, kaizhang@cityu.edu.hk

applications. Remarkably, their light manipulative properties at the nanoscale make them particular members of any advanced optoelectronics devices. Ultrathin 2D MXenes are further characterized by remarkable versatility in their advantageous properties, contributing significantly to their attractiveness in various research and application fields.

Touch screens, touch panels, and smart windows also come under their application domain due to their transparent conducting character. Adding mechanical flexibility to their transparent conduction makes them versatile 2D materials for soft-electronic gadgets in human–machine interface areas. Atomically thin stacked 2D MXene layers can be delaminated into single or few-layered MXenes with outstanding electrical and transparency characteristics, hence MXene transparent conductors. These electrical conductivity properties can be easily tuned by engineering the surface functional groups and lateral flake size variations [14, 15]. In a recent work [16], ultrahigh-molecular-weight polyethylene/MXene (UHMWPE) films were shown to rapidly heat up to 65 °C under 400 mW·cm^{-2} light irradiation while maintaining over 85% visible-light transmittance and a low haze of less than 12%. This demonstrates their significant potential for use in MXene-based transparent devices for energy and environmental applications. The only issue is avoiding the multilayer MXene, which brings downside opacity to its transparency characteristics. Ultradrawn UHMWPE-based 2D graphene composite demonstrated < 70% optical transparency following the trend of transparent 2D MXene [17]. Spray-coated various thickness-based $Ti_3C_2T_x$ MXene forms were fabricated and found under similar conditions with higher electrode transparency than graphene, carbon nanotube (CNT), and other composites. It was claimed that a 2.5-nm-thick film can exceed 90% transmittance ability [18]. The plasmonic behavior where the light interacts on the collective oscillation of free electrons and the ability to change the optical transparency through an ionotronic approach is attributed to the MXene's transparency. The atomic-scale thickness of these 2D materials not only contributes to a remarkable degree of mechanical flexibility but also facilitates a high level of optical transparency, which is a highly desirable attribute in many applications. Furthermore, the essential characteristics of MXene materials, such as the inherent electronic conduction, the interaction of MXene flakes with electromagnetic radiation, and the mechanical response, particularly the optoelectronic properties of an individual MXene flake, remain inadequately elucidated within the MXene scientific community to challenge the MXene transparent conduction.

A substantial body of in-depth literature review articles on MXenes indicates the significant attention this 2D nanomaterial class garners across various scientific disciplines, including materials synthesis, chemical process, and solid-state physics, owing to their appealing properties in numerous applications and the intriguing chemical and physical phenomena arising from their well-aligned layered 2D structure [1, 19–23]. Commencing with a concise examination of the synthesis and fabrication processes of MXenes, this review article explores their impact on the material's structure and surface chemistry associated with the transparent MXene materials. Subsequently, this review outlines the key findings of the transparent MXene applications. Each segment also deliberates on potential experimental and computational endeavors that could further unravel the electronic and optical attributes of transparent MXenes. The overall review is summarized in Fig. 1.

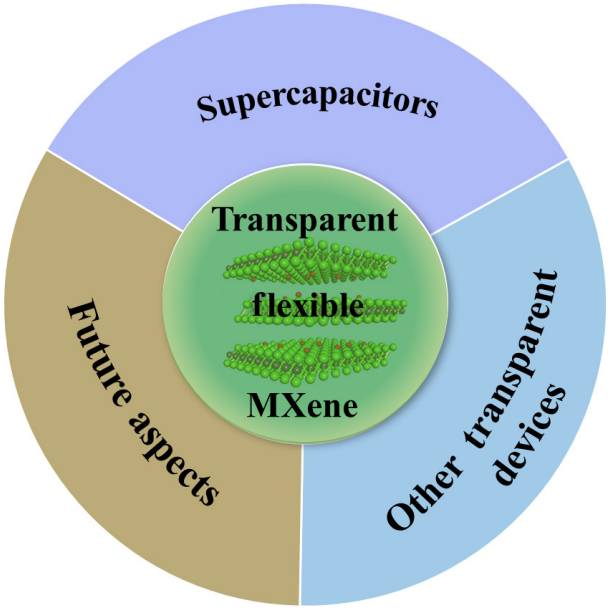

Figure 1 Overview of the transparent MXene-based review.

2 Transparent MXenes for supercapacitors

Over the past decade, there has been substantial progress in the development of flexible transparent supercapacitors (FTSCs), driven by their advantageous device configuration, swift charge/discharge capabilities, high energy and power density, and enduring operational stability [24, 25]. Unlike traditional supercapacitors, FTSCs are ideally suited for the rapid advancement of next-generation flexible transparent electronics, such as mobile intelligent devices, wearable artificial e-skins, health monitors, and miniaturized touch sensors [26–28]. The development of electrode materials with superior mechanical strength, high electrical conductivity, exceptional optoelectronic properties, and robust electrochemical performance is essential for developing flexible transparent conductive electrodes (FTCEs) [29, 30]. The integration of high-performance FTCEs into FTSCs represents a crucial technological advancement for the burgeoning field of flexible, transparent portable electronics [31, 32].

All-solid-state FTSCs are composed of four essential components: (i) the current collector, (ii) active electrode material, (ii) solid-state gel electrolyte, and (iv) substrate, all of which must exhibit both flexibility and transparency [33, 34]. The integrated assembly of the current collector, substrate, and active materials is known as the electrode [35, 36]. FTSC can be categorized into two primary types based on electrode configuration: film-supercapacitors [37, 38] (Fig. 2(a)) and micro-supercapacitors (MSCs) [37, 39, 40] (Fig. 2(b)). Film-supercapacitors are characterized by a traditional sandwich structure, which consists of two FTSC layers with solid-state gel electrolytes acting as separators. Symmetrical FTSCs arise when both electrodes are identical, whereas asymmetric FTSCs are constructed from a combination of two different electrodes [41]. In contrast, micro-supercapacitors feature solid-state gel electrolytes and two in-plane (IP) interdigital electrodes that cover the entire interdigital pattern area.

The flexibility of FTSC is paramount for their application in flexible devices, enduring primarily two forms of mechanical deformation: stretching and bending (Fig. 2(c)). Bending deformation can be subdivided into three distinct types: convex, concave, and a hybrid state that combines convex, release, and

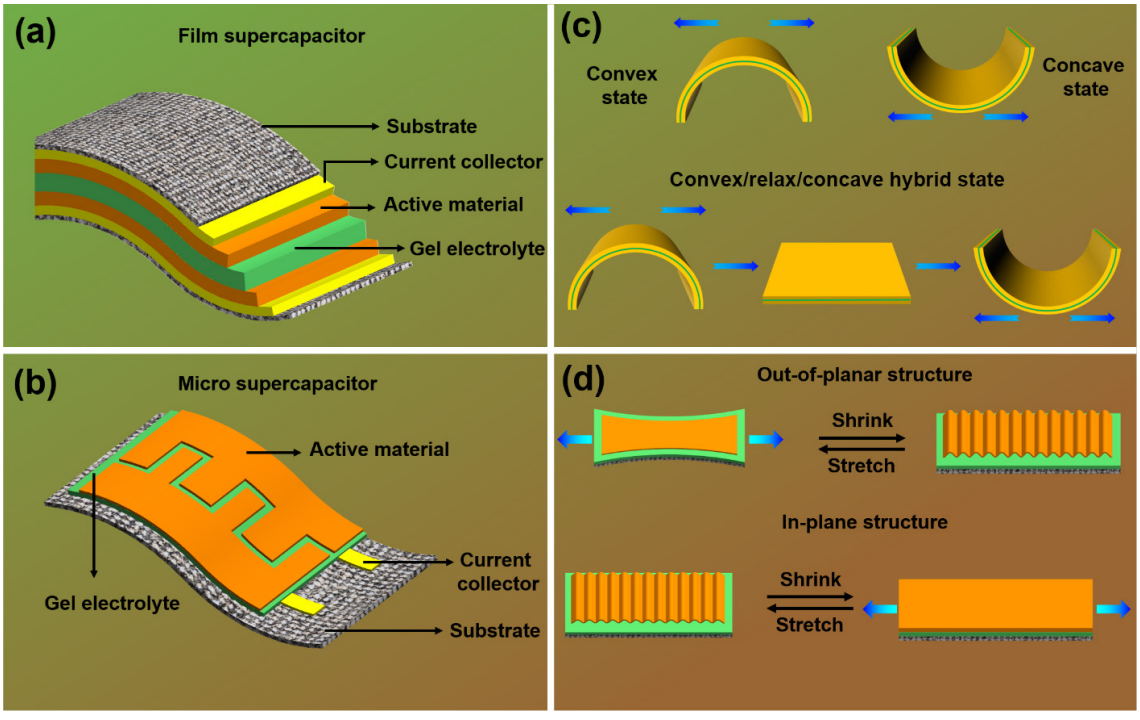

Figure 2 Graphical illustrations of transparent flexible electrode supercapacitor device configurations. (a) Co-facial film supercapacitor. (b) In-plane structure of micro supercapacitor. (c) Different classes of bending deformations in FTCE. (d) Different stretching states of FTSCs.

concave phases, depending on the bending curvature radius (r) [42]. When FTCEs are bent at angles ranging from 0° to 180°, the active materials may shift from their original positions due to mechanisms such as sliding, fracturing, or detachment from the substrate [43]. This displacement theoretically impacts the capacitive and optoelectronic properties. To address this, significant efforts have been made to preserve these properties across various applied voltages and multiple bending cycles, ensuring both electrical and mechanical stability.

Stretchability represents another crucial parameter for evaluating the flexibility of FTSC (Fig. 2(d)). Stretchable FTSC are designed to maintain their optoelectronic and electrochemical performance while undergoing mechanical elongation deformation ($\Delta L/L_0$), where ΔL represents the change in length and L_0 is the initial length of the FTCEs [44]. The stretchability largely depends on the materials used in the FTCEs, including flexible transparent films and substrates (e.g., polydimethylsiloxane), which must withstand significant strain without substantial structural failure. Stretchable FTCEs are engineered into two structural configurations: out-of-plane (OP) and IP. The OP structure involves depositing conductive active materials onto pre-stretched elastic substrates, which, upon relaxing to their original length, create a periodic wavy film on the substrate. The optoelectronic properties of OP FTCEs can be modulated by altering the buckling wavelength and amplitude [45, 46]. In contrast, the IP structure consists of transferring wrinkled thin films onto resilient substrates. During stretching, the films flatten and revert to their initial wrinkled state when the electrode returns to its original length [47]. These structural designs enhance the potential of stretchable FTSCs for integration into power-efficient wearable electronics.

MXenes ($M_{n+1}X_nT_x$) are prepared by selectively extracting the "A" layer from their parent MAX phases, leading to the formation of multi-layered (m-)MXenes. The "ene" suffix denotes their two-dimensional nature, similar to graphene [48]. The M–A bond in MAX phases is weaker and more reactive than the M–X bond, making it prone to cleavage, which is crucial for MXene synthesis. During the etching process, surface terminations (T_x) rapidly form on the exposed "M" atoms to preserve charge neutrality. This results in metallic properties, as the 3d states of the outer M(1) atoms transition into delocalized metallic-like bonding states around the Fermi level following the cleavage of M–A bonds. This metallic bonding, particularly pronounced in the outer M(1) atoms compared to the inner M(2) atoms, imparts exceptional electrical conductivity and mechanical flexibility, while minimizing interface tunneling junctions and barriers [49–52]. Moreover, MXene colloidal exhibits unique properties of hydrophilicity, viscosity, and colloidal stability, which facilitate the preparation of MXene-based FTCEs. Their metal oxide-like redox-active surfaces and inherent high metallic conductivity make MXenes particularly well-suited for pseudocapacitance-driven energy storage, offering a theoretical capacity of 615 C·g^{-1} or 1200 F·g^{-1} [53, 54]. Consequently, MXenes are anticipated to serve effectively as both conductive current collectors and electrochemically active materials in FTCEs.

Halim et al. [55] pioneered the creation of transparent conductive 2D MXene thin films using direction current (DC) magnetron sputtering within an ultrahigh vacuum system, introducing a novel top–down approach for fabricating transparent MXene films. The film demonstrated an electronic conductivity ranging from 2000 to 5000 S·cm^{-1} and tunable transmittance ranging from 14% to 85%, depending on thickness. Thicker films tended to have lower optical transmittance, while thinner films demonstrated decreased conductivity. Nonetheless, the high deposition temperature of 780 °C posed challenges for large-scale production. Balancing transparency with sheet resistance (R_s) is crucial for optimizing the performance of transparent and conductive Ti_3C_2 films. The solution-processing techniques—such as spin-coating, dip-coating and spray coating—offer a simple, cost-effective, and environmentally

friendly method for fabricating Ti_3C_2 FTCEs through layer-by-layer deposition of Ti_3C_2 dispersions onto flexible transparent substrates.

For instance, Ren et al. [56] demonstrated the fabrication of a conductive $Ti_3C_2T_x$/poly(3,4-ethylenedioxythiophene):polystyrenesulfonic acid (PEDOT:PSS) hybrid flexible transparent electrode for supercapacitors using the spin-coating technique and the fabrication process is shown in Figs. 3(a) and 3(b). The prepared $Ti_3C_2T_x$ nanosheets were further exfoliated to smaller dimensions, which enabled the formation of a homogeneous and interconnected $Ti_3C_2T_x$/PEDOT:PSS composite film with enhanced redox activity and accelerated ionic transport. $Ti_3C_2T_x$ nanosheet dispersion was mixed with PEDOT solution in varying mass ratios from 0:1 to 2.5:1.0, yielding a stable $Ti_3C_2T_x$/PEDOT hybrid dispersion in deionized (DI) water. Spin coating was used to deposit pure PEDOT and $Ti_3C_2T_x$/PEDOT composites onto graphene films on polyethylene terephthalate (PET) substrates. The films were then annealed at 120 °C for 20 min in ambient air. Prior to the spin coating, the graphene film was prepared by chemical vapor deposition, which exhibited 86.5% optical

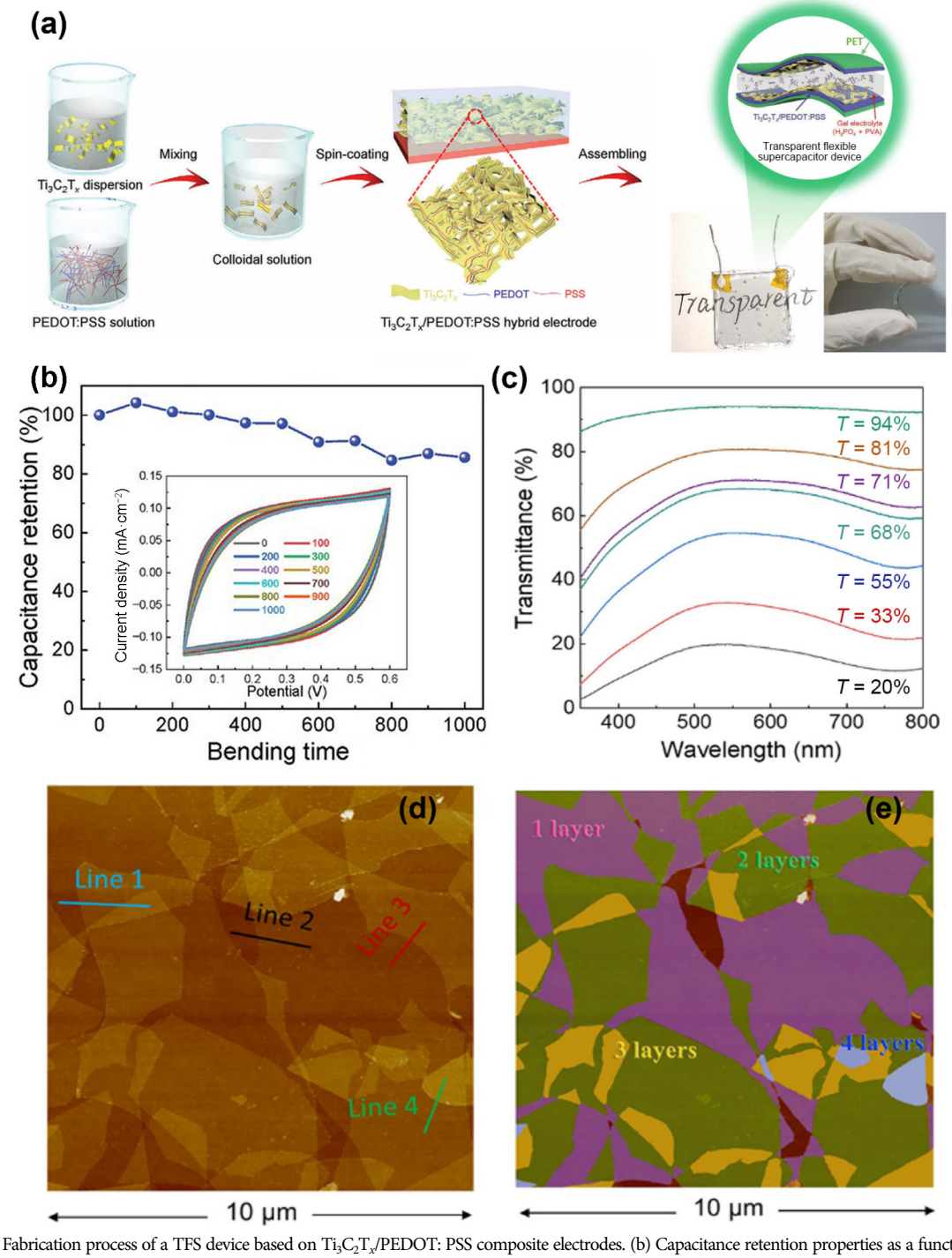

Figure 3 (a) Fabrication process of a TFS device based on $Ti_3C_2T_x$/PEDOT: PSS composite electrodes. (b) Capacitance retention properties as a function of repetitive bending times at a bending radius of 1.0 mm (inset: CV curves at 100 mV·s^{-1} before and after repetitive bending to 1 mm for different times). Reproduced with permission from Ref. [56], © Wiley-VCH GmbH 2024. (c) Optoelectronic property of $Ti_3C_2T_x$ using UV–vis spectra of flexible transparent films with various transmittance. (d) Atomic force microscopy (AFM) image of a $Ti_3C_2T_x$ film at T = 94% (MXene coverage 98%). (e) Comparison of different numbers of layers in AFM region with different colors. Reproduced with permission from Ref. [57], © Guo, T. Z. et al. 2023.

transparency at 550 nm and a R_s of 100 Ω·sq^{-1}, making it suitable as a current collector for FTSCs. In contrast, Guo et al. [57] experienced $Ti_3C_2T_x$ MXene inks for transparent conductive electrodes. Their results demonstrated that a film with 96.7% transparency achieved a sheet resistance (R_s) of 800 Ω·sq^{-1}, markedly lower than that of other MXene-based transparent conductive electrodes (Fig. 3(c)). At a transparency level of 94%, large single-layer flakes were able to form continuous conductive networks with 98% coverage, effectively mitigating percolation issues (Fig. 3(d)). This lack of percolation problems contributes to the films' superior optoelectronic properties. The average film thickness, within a 10 μm × 10 μm area, is around 1.8 layers, or approximately 2.2–2.7 nm, based on a thickness of 1.2–1.5 nm per layer (Fig. 3(e)).

A comparison between the studies by Ren et al. [56] and Guo et al. [57] highlights the significant impact of $Ti_3C_2T_x$ MXene film thickness on its optical characteristics. With increasing film thickness, a noticeable reduction in ultraviolet (UV) transmittance is observed. To further investigate charge-transport mechanisms within MXenes. Nguyen et al. [58] conducted a density functional theory (DFT) analysis on a flexible, transparent MXene-based ultrafast photodetector ($ZnO/Ti_3C_2(OH)_2$/indium tin oxide (ITO)). Their analysis revealed an interlayer spacing of 2.5 Å at the ZnO/ITO interface, while the $ZnO/Ti_3C_2(OH)_2$ and $Ti_3C_2(OH)_2$/ITO interfaces exhibited interlayer spacings of 1.9 and 1.7 Å, respectively (Figs. 4(a)–4(c)). The electronic band structure analysis demonstrated numerous bands crossing the Fermi level in the $ZnO/Ti_3C_2(OH)_2$/ITO configuration, unlike the ZnO/ITO configuration, signifying strong intrinsic metallicity in the former (Figs. 4(d) and 4(e)). The incorporation of $Ti_3C_2(OH)_2$ MXene at the ZnO/ITO interface introduced multiple linear band dispersions near the Fermi level, characterized by carriers with low effective mass and high group velocity, thereby enhancing electrical conductivity.

Thus, the intrinsic metallicity and linear band dispersions near the Fermi level in the $ZnO/Ti_3C_2(OH)_2$/ITO structure provide an enhanced charge-transport channel. This strong charge-transport capability, coupled with high electrical conductivity, suggests that $Ti_3C_2(OH)_2$ MXene is a promising candidate for energy storage applications, particularly in devices where efficient charge transfer and storage are critical.

In 2024, M. Y. Jung et al. [59] reported a significant advancement in transparent supercapacitor technology through the development of a networked MXene/nickel-cobalt layered

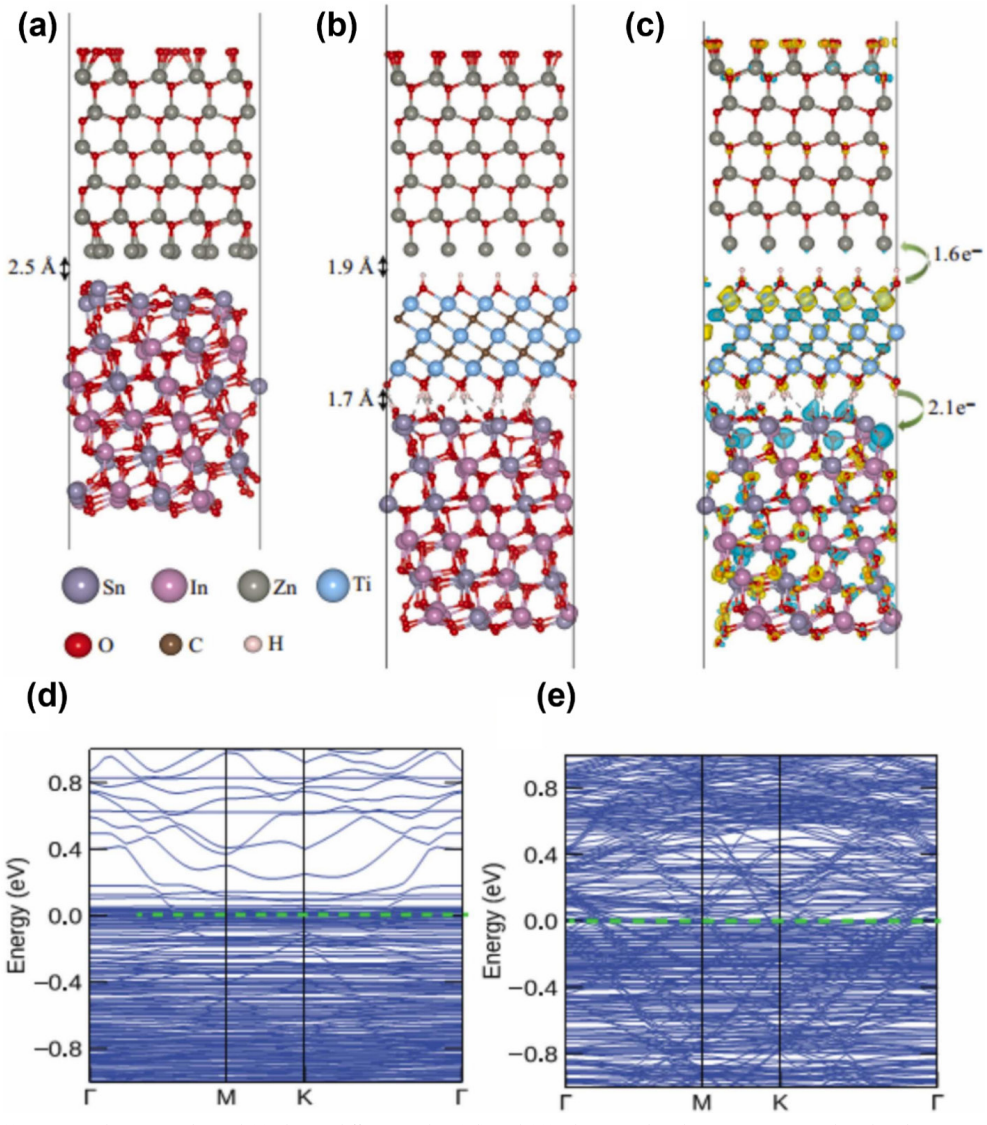

Figure 4 ((a) and (b)) Optimized DFT results and (c) charge difference plot. ((d) and (e)) Electronic band structures. Reproduced with permission from Ref. [58], © Elsevier Ltd. 2023.

double hydroxide (LDH) (MX/NCOH) composite designed for high-performance transparent electrode applications. The synthesis, as detailed in their study, involved optimized conditions, including a 100 s NCOH deposition followed by a 20 min immersion in a negatively charged MXene colloidal solution (Fig. 5(a)). This approach yielded a unique architecture with intricately intertwined MXene sheets that bridged the walls of the NCOH-100 layer, forming a conductive network that enhanced

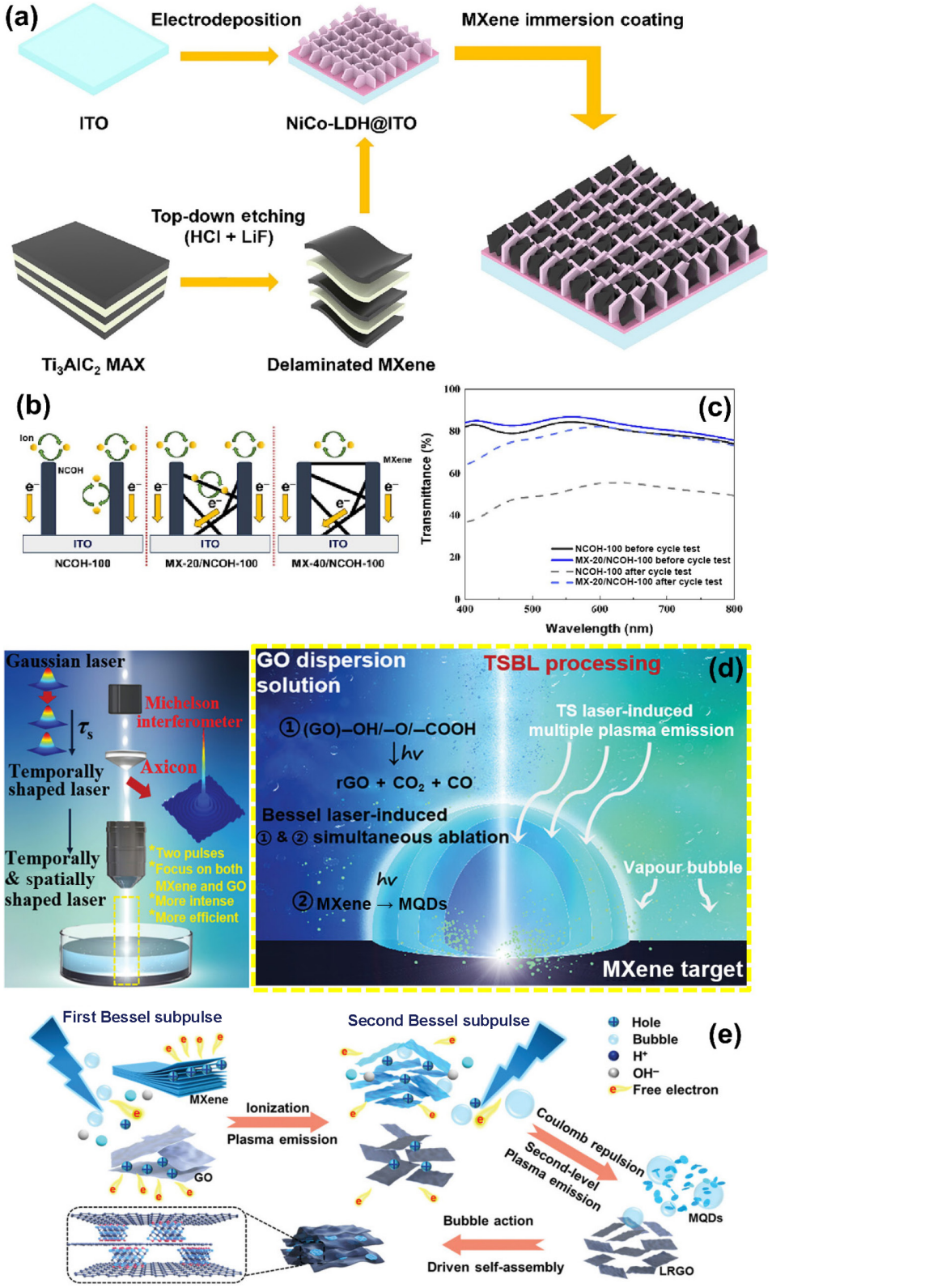

Figure 5 Schematic illustration of (a) MXene coated NiCo-LDH supercapacitor electrode fabrication process, (b) the energy storage mechanism, (c) corresponding transmittance of NCOH-100 and MX-20/NCOH-100. Reproduced with permission from Ref. [59], © Elsevier B.V. 2024. Schematic illustration of (d) mechanism and light field simulation images of temporally and spatially shaped laser and formation process of MQD/laser rGO (LRGO), (e) reaction mechanism and process of TSBL processing the MQD/LRGO composites. Reproduced with permission from Ref. [60], © Wiley-VCH GmbH 2022.

electron and ion transport. This structure was identified as critical for improving the electrochemical performance of the composite supercapacitors. The charge storage mechanisms of NCOH-100, MX-20/NCOH-100, and MX-20/NCOH-100 composites were also investigated, revealing that NCOH-100 relies on rapid and reversible redox and pseudocapacitive reactions occurring on the surfaces of its wall-like nanosheets (Fig. 5(b)). The inclusion of networked MXene nanosheets facilitated electron conduction and maintained pseudocapacitive reactions by improving ion transport. However, excessive MXene loading within the NCOH-100 framework created diffusion barriers, impeding reactive ion transport and reducing pseudocapacitive efficiency. The optical performance was further evaluated, with transmittance values of 86.7% for MX-20/NCOH-100 and 86.4% for NCOH-100 at 550 nm, showing comparable transparency. Over 7000 stability cycles, the transmittance of MX-20/NCOH-100 decreased only to 80.1%, whereas NCOH-100 experienced a significant reduction to 51.4%, demonstrating superior structural and optical stability in MX-20/NCOH-100 (Fig. 5(c)) [59].

Similarly, L. Jiang et al. developed MXene quantum dots/graphene oxide (MQD/GO) composites for transparent supercapacitors using an ultrafast shaped laser-induced method. This innovative approach utilized temporally and spatially shaped femtosecond lasers to irradiate an MXene target suspended in GO, enabling simultaneous GO reduction and MXene exfoliation (Figs. 5(d) and 5(e)). A temporally shaped Bessel laser (TSBL) was employed to focus its strongest energy on the MXene target, inducing Coulomb interference and first-level photoexfoliation, resulting in the production of uniform MQDs. Weaker laser fields facilitated GO reduction via multiphoton ionization and oxygen atom removal. Subsequent laser pulses promoted secondary plasma emission and further photoexfoliation, aided by Coulomb repulsion and ionization-induced charge accumulation. Plasma decay led to cavitation bubble formation, homogenizing the MQD size and enhancing their dispersion in reduced GO (rGO). The shaped femtosecond laser process achieved high-quality MQDs with uniform morphology, attributed to enhanced ionization of water molecules and increased light absorption during successive pulses. This efficient one-step synthesis highlights the potential of advanced laser-based methods for fabricating next-generation materials for energy storage applications [60].

Optimizing the device configuration and electrode architecture is crucial for achieving peak electrochemical performance of the selected electrode materials. Couly et al. [61] demonstrated an asymmetric flexible micro-supercapacitor based on MXene-rGO, as illustrated in Figs. 6(a) and 6(b). The device was fabricated using both co-facial and coplanar arrangements of 2D rGO and $Ti_3C_2T_x$ layers. In the co-facial design (Fig. 6(a)), the MXene and rGO layers are aligned within the same plane, whereas in the coplanar configuration (Fig. 6(b)), the layers are positioned facing each other, with a poly(vinyl alcohol) (PVA)/H_2SO_4 gel electrolyte acting as the separator.

The electrochemical analysis of the fabricated device revealed an even distribution of the cell voltage window, with the negative electrode ($Ti_3C_2T_x$) operating from 0 to 0.5 V and the positive electrode (rGO) operating from 0.5 to 1 V in cyclic voltammetry (CV) analysis (Fig. 6(c)). Additionally, the CV curves of the asymmetric micro-supercapacitor exhibited a quasi-rectangular shape, likely due to the pseudocapacitive nature of the MXene electrode. For the symmetric $Ti_3C_2T_x$ interdigitated micro-supercapacitor, a maximum voltage window of 0.6 V was achieved, highlighting the narrow voltage window characteristic of the symmetric configuration. The Ragone plot provided a comparative analysis of the co-planar and co-facial electrode architectures, showing a pronounced decline in performance for the co-facial configuration at high scan rates, which can be attributed to the less favorable architecture (Fig. 6(d)).

For instance, Zhang et al. [62] developed a sandwich-type MXene-based transparent flexible solid-state supercapacitor device, demonstrating remarkable longevity, high transparency, and superior energy and power densities, as shown in Fig. 7(a). The transmittance spectra for both a single electrode and the symmetric device revealed an optical transparency of approximately 80% for the latter Fig. 7(b). This level of transparency significantly exceeds that of other reported supercapacitor devices, such as those using cellulose nanofiber/rGO (56%), wrinkled graphene (60%), or graphene film (69%). The device exhibited a rapid charge/discharge response upon voltage reversal and sublinear galvanostatic charge/discharge (GCD) curves, indicating highly capacitive behavior and excellent power handling properties (Fig. 7(c)). Moreover, the asymmetric device demonstrated outstanding long-term cycling stability, with capacitance gradually increasing over 20,000 cycles and a Coulombic efficiency of 100% (Fig. 7(d)). The increased capacitance is likely due to improved access to deep interlayer sites between MXene sheets, enhancing the availability of active sites for capacitive charge storage during cycling.

The $Ti_3C_2T_x$/PEDOT hybrid flexible transparent electrode, as reported by Ren et al. [56] and Zhang et al. [57], it is evident that the thickness of the $Ti_3C_2T_x$ MXene film significantly influences the film's optical properties. As the thickness of the film increases, its transmittance in the UV region decreases. To elucidate the charge-transport channels in MXene, Nguyen et al. [58] performed a density functional theory analysis on a flexible and transparent MXene-based ultrafast photodetector (ZnO/$Ti_3C_2(OH)_2$/ITO). They found the interlayer spacing at the ZnO/ITO interface to be 2.5 Å, while the ZnO/$Ti_3C_2(OH)_2$ and $Ti_3C_2(OH)_2$/ITO interfaces had interlayer spacings of 1.9 and 1.7 Å, respectively (Figs. 4(a)–4(c), DFT). The electronic band exhibits remarkable mechanical flexibility under stringent conditions. With a bending radius of 1.0 mm, the device retains stable electrochemical performance, showing only a 4.0% loss in capacitance. Furthermore, after 1000 bending cycles at this radius, the capacitance retention exceeds 86% of the initial value, underscoring its exceptional bending durability (Fig. 3(b)). These outstanding characteristics are attributed to the innovative $Ti_3C_2T_x$/PEDOT composite matrix, which adeptly manages bending stresses. The comprehensive insights from the results of various flexible transparent MXene electrodes underscore the potential of highly transparent and conductive MXene-based materials in advanced energy storage systems, paving the way for future developments in high-performance supercapacitors and batteries.

From a fundamental perspective, these findings highlight the potential to engineer transparent films using metallic 2D materials that offer an exceptional balance of optoelectronic performance and flexibility-something that is often difficult to achieve with conventional transparent electrodes, which tend to compromise either flexibility or conductivity. On the practical side, the approach employed is not only simple but also cost-effective, promoting sustainability. The demonstrated prototype performance and volumetric capacitance underscore the promising potential of flexible $Ti_3C_2T_x$ films for a variety of applications, including displays, touch screens, organic solar cells, wearable electronics, and transparent energy storage devices. In

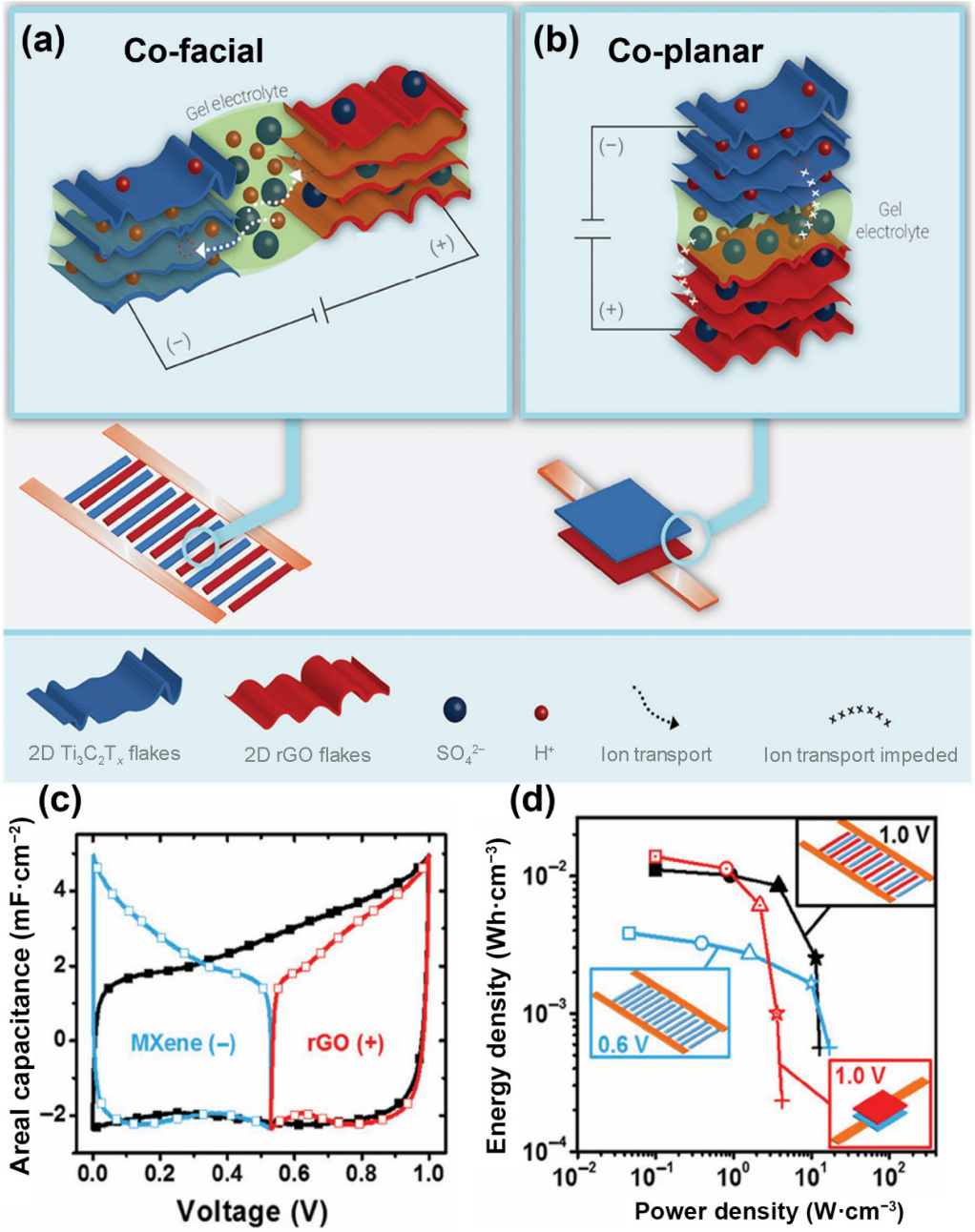

Figure 6 ((a) and (b)) Schematic illustrations of asymmetric FTSCs, (c) CVs of the MSC and the individual electrodes recorded at 2 mV·s^{-1}, and (d) Ragone plot of FTSCs. Reproduced with permission from Ref. [61], © WILEY-VCH Verlag GmbH & Co. KGaA, Weinheim 2017.

another study [59], MXene nanosheets were introduced into a NiCo-LDH, resulting in enhanced stability and electrochemical properties while retaining high transparency. A transparent symmetric supercapacitor (Fig. 7(e)) using MXene-coated NiCo-LDH exhibited strong performance, with a power density of 120.00 μW·cm^{-2} at an energy density of 2.23 μWh·cm^{-2} along with excellent capacitance retention of 85.9% after 9000 charge–discharge cycles. Such MXene-based devices and composites hold significant promise for transparent supercapacitor applications. The summary of FTSC device is displayed in Table 1.

3 Other applications of transparent MXenes

MXenes have undoubtfully revolutionized the family of 2D materials attributed to their unique properties. The rapid and state-of-the-art progress from synthesis of MXenes to their various applications proved their strong potential as emerging material. Currently, the rising consumer demand for portable and light-weight devices introduced the focus of research towards development of transparent MXenes. Therefore, efforts have been invested to design transparent MXenes with high optical transparency, which is based on high figure-of-merits (both electrical and capacitive, i.e. FoM_e, FoM_c). Whereas, the FoM_e and FoM_c evaluate the power output and energy storage capabilities of transparent MXenes [66].

In case of transparent MXenes as electrodes (with or without transparent substrate), the MXene (film/electrode) thickness control is crucial to design efficient transparent electrode or device. The fabrication of transparent electrode requires high precision as percolation effect dominates while thinning the film leading to poor electrochemical performance and optoelectronic

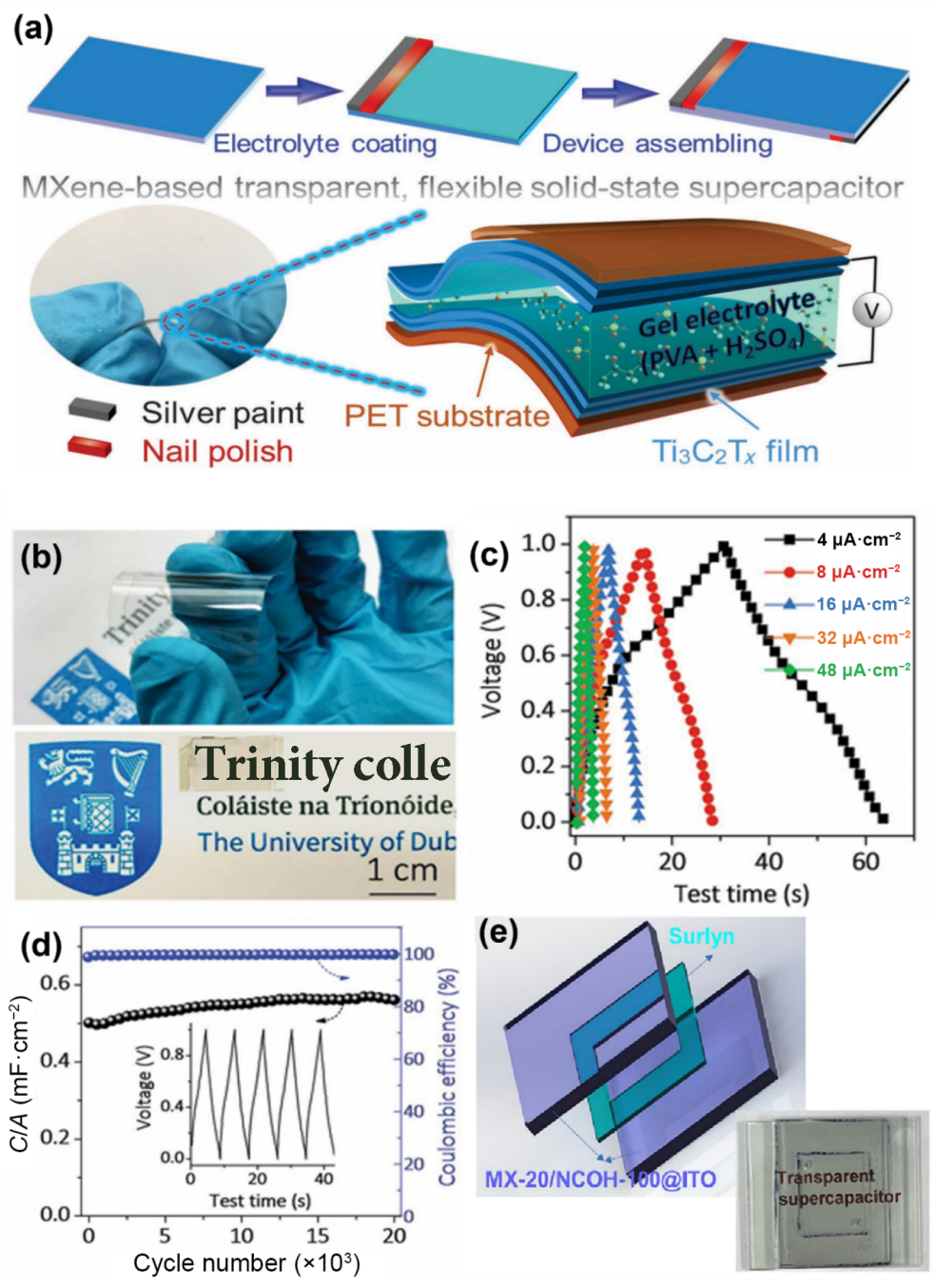

Figure 7 (a) Schematic representation of $Ti_3C_2T_x$ MXene-based FTSC fabrication. (b) Digital images of FTSC, (c) GCD, and (d) durability of the asymmetric FTSC device the asymmetric device. Reproduced with permission from Ref. [62], © WILEY-VCH Verlag GmbH & Co. KGaA, Weinheim 2017. (e) Pictorial representation of MX-20/NCOH-100@ITO symmetric device. Reproduced with permission from Ref. [59], © Elsevier B.V. 2024.

properties. However, MXenes have shown low percolation issues when fabricating advanced transparent electrodes and devices [67]. To date, numerous methods have been adopted to fabricate the MXene-based transparent conductive electrodes. For instance, Fig. 8(a) shows a blade coating technique was adopted to produce transparent $Ti_3C_2T_x$ MXene electrode (transmittances (T) = 83.4%). The $Ti_3C_2T_x$ ink consistency was maintained in 2 to 10 mg·mL^{-1} range, ensuring high transparency and thickness (6.7 nm) of $Ti_3C_2T_x$ MXene film. The utility of large sized $Ti_3C_2T_x$ flakes (12.2 μm) assisted the high FoM_e due to reduced interface junctions for electron hopping. In addition, the high electronic conductivity (19,325 S·cm^{-1}) of transparent $Ti_3C_2T_x$ electrode also aided the low percolation problem [57]. M Ebrahimi et al. [68] developed $Ti_3C_2T_x$ transparent conductive electrode using spin coating technique. The transparent conductive $Ti_3C_2T_x$ electrodes were prepared at different spinning speeds of 1000 to 4000 rpm. Significantly, it was observed that an increase in thinning of MXene film for high transparency (72% to 94%) caused an increased sheet resistance (2010 to 23,660 Ω·sq^{-1}). This resistance can be caused by high defects and small sheet size. Similarly, the inkjet printing method was adopted to design transparent $Ti_3C_2T_x$ MXene film with high FoM (optical conductivity) 0.0012 to 0.13 [63]. Transparent V_2CT_x MXene films have also been reported with transmittance of 89% [69].

Interestingly, the transparent MXene electrode such as $Ti_3C_2T_x$ possess active response towards the field driven MXene electronics

Table 1 Summary of the FTSC devices

Electrode material	Gel electrolyte	T (λ)	Potential window (V)	Capacitance	Energy density	Power density ($\mu W \cdot cm^{-2}$)	Flexibility	Cycle stability (retention @cycles)	References
$Ti_3C_2T_x$	PVA/H_2SO_4	80% (550 nm)	0.6	0.86 mF·cm^{-2} (2 μA·cm^{-2})	—	—	—	95%@24,000	[62]
$Ti_3C_2T_x$// SWCNT	PVA/H_2SO_4	72% (550 nm)	1.0	1.6 mF·cm^{-2}	0.05 μWh·cm^{-2}	—	—	No capacitance decay over 20,000	[62]
$Ti_3C_2T_x$	PVA/H_3PO_4	73% (550 nm)	0.4	192 μF·cm^{-2} (2 mV·s^{-1})	0.0043 μWh·cm^{-2}	0.077	180° bending (100.8%)	100.8%	[63]
MXene quantum dots/laser reduced graphene oxide	PVA/H_2SO_4	90%	1.2	10.42 mF·cm^{-2}	2.04 × 10^{-3} mWh·cm^{-2}	129.4	180° bending	97.6% @12,000 cycles	[60]
MXene/ NiCo-LDH	1 M KOH	80.1%	2.4	136.9 F·cm^{-2}	2.23 μWh·cm^{-2}	120.00	—	85.9% @9000 cycles	[59]
PEDOT:PSS/Ag NFs/NOA_{63}	PVA/H_2SO_4	77.4% (550 nm)	1.0	0.91 mF·cm^{-2} (5 mV·s^{-1})	0.09 μWh·cm^{-2}	74.1	r = 2 mm bending for 5000 cycles (98.5%)	95%@10,000	[64]
MXene quantum dots/laser reduced graphene oxide	PVA/H_2SO_4	90%	1.2	10.42 mF·cm^{-2}	2.04 × 10^{-3} mWh·cm^{-2}	129.4	180° bending (100%)	97.6%@12,000	[60]
$Ti_3C_2T_x$	PVA/H_3PO_4	87% (550 nm)	0.4	187.5 μF·cm^{-2} (@10 mV·s^{-1})	—	—	180° bending (100.8%)	85%@10,000	[63]
Zn-$Ti_3C_2T_x$	$ZnSO_4$-PAM hydrogel	94% (550 nm)	1.2	318 μF·cm^{-2} (5 mV·s^{-1})	0.0513 μWh·cm^{-2}	103	120° bending (99%)	76%@10,000	[65]

applications. However, the high electrical conductivity and optical transparency are affected by several environmental factors. Therefore, the environmental stability of transparent MXene electrode has been maintained by thin polymer lamination of these electrodes efficiently used in light-emitting diode (LED) displays, triboelectric nanogenerators (TENG) and sensors [70]. J Liu et al. [71], reported the fabrication of TENG designed by MXene-Ag nanowires (AgNW) with polyurethan nanofiber matrix (MAMP) electrode. The electrode displayed significant transmittance of 87.6% with very low resistance of 10.1 Ω·sq^{-1}. The prepared TENGs were integrated as wearable sensor to access the pressure. The real-time output signals were detected from pressure sensor, against the applied force to TENG, as shown in Fig. 8(b). Based on the variation of contact area with TENG, different voltages were produced and detected in the 3 × 3 sensor array. Therefore, transparent MXenes benefits of portable and wearable devices.

Moreover, there is an increased demand for light-weight, low-cost, flexible and advanced electronic and photovoltaic applications. MXenes, due to their unique traits, have been employed to fabricate transparent electrode for solar cells. The high conductivity of MXene was merged with Ag-nanowires-poly(urethane acrylate) (PUA) to produce transparent and flexible film (Fig. 8(c)) through slot-die coating technique revealed the high FoM (162.49). The transparent photovoltaic solar cell retained 84.6% of initial power conversion efficiency (PCE) after 1000 bending/unbending cycles of 5 mm bending radius [72]. The remarkable performance proved the potential of transparent MXene-based films in the photovoltaic applications.

On the other hand, S Kumar et al. [73], reported the fabrication of transparent MXene electrode by spin coating $Ti_3C_2T_x$ MXene onto polyethylene terephthalate transparent substrate Fig. 9(a). A transmittance of 87% was achieved with a sheet resistance of 424 Ω/sq annealed at 170 C. In addition, the flexibility of transparent MXene electrode was investigated by employing Scotch-tape peeling method. The mechanical properties of the unheated and heat-treated samples were analysed by tape peeling four times, as shown in Fig. 9(b). The study demonstrated an increase in the sheet resistance for the unheated electrodes where the reason is the loss of adhesion of the MXene layers. In contrast, the heated samples at 100 and 170 C were more stable with an increase of sheet resistance up to 15% for transparent MXene film annealed at 170 C. Figure 9(c) illustrates the transparent conductive MXene electrode when incorporated as polymer dispersed liquid crystal (PDLC) smart window. The transmittance was recorded with voltage range from 0 to 60 V and showed maximum transparency of 80% at 60 V in "ON" state while opaque at "OFF" state.

The transparent MXene conductive electrode has also been explored for light-emitting diodes. The precise surface engineering of solution processed $Ti_3C_2T_x$ MXene used as transparent conductive MXene anode (work function 5.1 eV) revealed equivalent results compared to conventional ITO (work function 4.8 eV). The green phosphorescent organic LED (phOLED) was designed using transparent $Ti_3C_2T_x$ MXene and showed high luminescence at applied voltages with a quantum efficiency of 28.5% photon–electron conversion efficiency and a current efficiency of 102.0 cd·A^{-1} (Figs. 9(d) and 9(e)). The high optoelectronic performance is attributed to MXene's higher hole-current density contributing to its high work function and overall performance [74]. Similarly, to further enhance the performance of quantum light-emitting diode, the MXene and silver nanowires (AgNW)-based hybrid transparent conductive electrode was reported. Whereas, the mechanical stability of the electrode was maintained by treating it with thin layer of poly methyl methacrylate (PMMA). Interestingly, controlling the amount of MXene in the hybrid transparent electrode results in desired work function for the efficient outcome. Moreover, the AgNW in transparent hybrid film assisted the low sheet resistance from electrode (13.9 Ω·sq^{-1}), increasing the transparency up to 83.8% [75]. Recent studies also reported the tailoring of transparent MXene conductive electrodes using bio-species such as plant

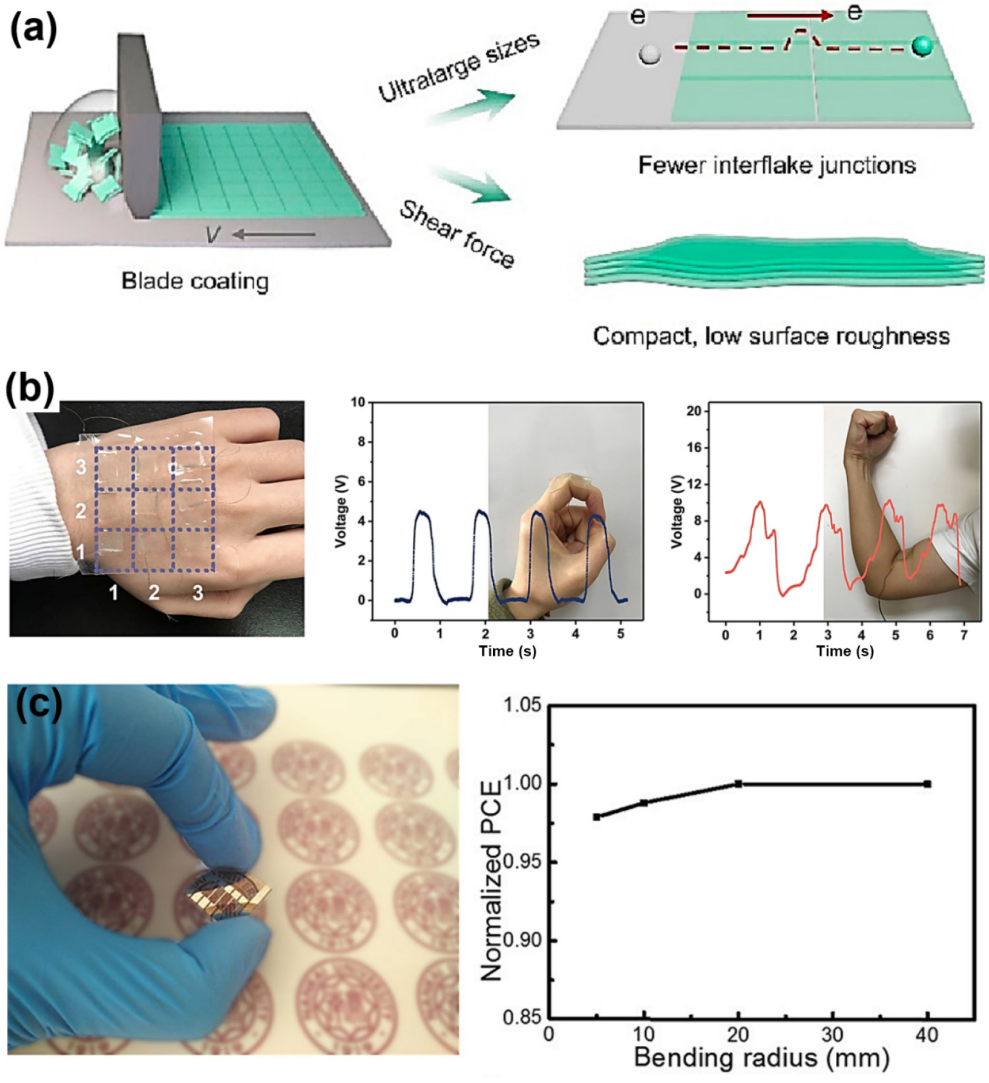

Figure 8 (a) Illustration of transparent MXene fabricated via blade-coating. Reproduced with permission from Ref. [57], © Guo, T. Z. et al. 2023. (b) Optical image of the sensor array (3 × 3) and output voltage signals under pressure of finger and arm. Reproduced with permission from Ref. [71], © Elsevier Ltd. 2020. (c) Flexible perovskite solar cell (PSC) and graph of normalized flexible PSCs with $Ti_3C_2T_x$ AgNW-PUA transparent electrodes at different bending radii. Reproduced with permission from Ref. [72], © American Chemical Society 2019.

leaves (Fig. 9(f)) and their utility as UV photodetectors with transparency as high as 90%. The transparent leaf electrode maintained a photocurrent of 90% after 1000 bending cycles with good photo response [76]. In summary, the unique and attractive traits of MXenes due to their enriched structural variability and easy tuneability nominated them as emerging candidate for wide range of applications. Nonetheless, the use of transparent conductive MXenes in various applications has also paved path to explore their potential as efficient transparent electrodes and their utility in the desired portable and wearable electronics.

4 Conclusion and future aspects

In conclusion, this review culminates with an overview of the challenges faced in this transparent MXene field and offers insights into future research avenues. The exceptional characteristics of high electrical conductivity, 2D morphology, solution processability, and excellent mechanical properties establish MXenes as up-and-coming contenders for transparent conductors in a range of applications. Despite the extensive research conducted on MXenes over the years, understanding these remarkable materials is still nascent. Many fundamental properties of MXenes remain uncharted territory, including the ongoing debate surrounding their surface terminations. Researchers can potentially construct hybrid and composite materials through the application of self-assembly techniques or by employing advanced additive manufacturing methods, thereby further expanding the horizons of 2D MXene's material science and engineering. We aspire that this review serves as a valuable compass for both theoreticians and experimentalists engaged in exploring the transparent MXene's electronic and optical characteristics of this relatively nascent yet rapidly expanding family of 2D nanomaterials. An inclusive understanding of transparent MXene and insights into future perspectives discussed below will be crucial in unlocking the full potential of MXene for real-world applications.

(1) Various film deposition techniques, such as magnetron sputtering, spray-coating, electrospraying, spin-casting, dip-coating, and interfacial film assembly, must be investigated in-depth as effective methods for producing transparent MXene thin films.

(2) A comprehensive knowledge regarding the plasmonic and

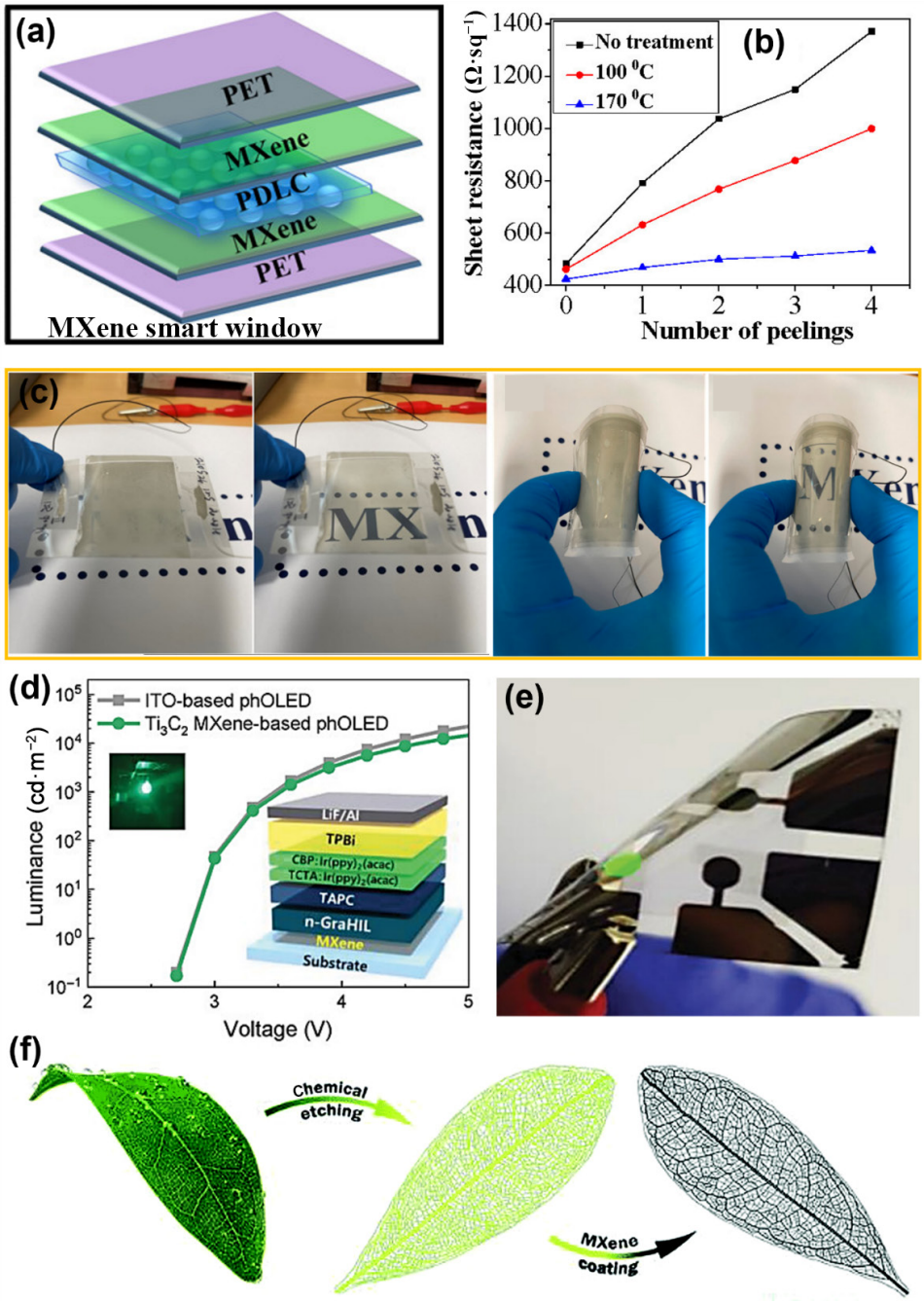

Figure 9 (a) Illustration of transparent MXene smart window. (b) Mechanical properties analysis graph of transparent MXene electrode untreated and treated at different temperature. (c) PDLC in OFF state (opaque). Reproduced with permission from Ref. [73], © American Chemical Society 2021. (d) PDLC ON state at 60 V. (e) OFF state in bending PDLC. Reproduced with permission from Ref. [74], © WILEY-VCH Verlag GmbH & Co. KGaA, Weinheim 2020. (f) ON state in bending PDLC. Reproduced with permission from Ref. [76], © The Royal Society of Chemistry 2020.

photonic properties of MXenes necessitates further research to uncover their full potential as transparent MXenes.

(3) The 2D structure of MXenes enables the formation of van der Waals heterostructures with other 2D materials, leading to intriguing electronic band properties that can be explored parallelly, leveraging their optical and plasmonic characteristics.

(4) Nitride and carbonitride MXenes are anticipated to exhibit more pronounced surface plasmon-related phenomena akin to bulk transition metal nitrides, highlighting the need for collaborative efforts between modeling and experimental studies to delve deeper into the plasmonic and photonic properties of transparent MXenes.

(5) The utilization of transparent MXenes in photothermal therapy applications must be expanded to understand the light-to-heat conversion systems.

(6) The formidable challenge for experimentalists in achieving uniform surface terminations in synthesized MXenes stands out as crucial for transparent MXene applications. It remained the unchartered territory.

(7) The pending task for the experimental realization of intrinsic MXene semiconductors, despite theoretical predictions using DFT, must be discussed for any transparent MXene applications.

(8) While the optical properties of transparent MXenes are

highly appealing, their interactions with electromagnetic waves are not fully understood, posing a significant challenge for their utilization in electromagnetic interference shieldings, nanophotonics, and plasmonic applications.

(9) MXenes have excellent electrical conductivity coupled with high hydrophilicity; however, they are prone to oxidation in extreme environments. More exploration is needed to produce less oxidized transparent MXenes for the aimed optoelectronic devices.

(10) To avoid MXene's oxidation susceptibility in the realm of transparent MXene applications in optoelectronic areas, it is recommended that the MXene nanosheets be assembled optimally into a high-performance nanocomposite.

(11) Diverse chemical treatments have the capacity to boost the work function and characteristics of MXene, facilitating enhanced device efficiency and stability while making photoactive substances in transparent electrodes, active components, and materials for electron and hole collection in solar cells.

(12) The challenges encountered by traditional electrochromic devices and their mechanisms are linked to inadequate electrical conductivity and degradation caused by reversible ion intercalation, problems that can be mitigated by incorporating transparent MXene with these components.

(13) The convergence of features like photothermal conversion efficiency, high thermal conductivity, and structural properties of MXene makes it a remarkable choice for harnessing the plasmonic effect for transparent MXene soft electronic devices.

(14) Manipulation of interfaces and the design of advanced heterostructures could emerge as practical approaches for improving the photoelectric and transparent characteristics of MXene-based photovoltaic solar devices.

(15) Ti-based MXenes are distinguished by their solution processability, high transmittance, figure of merit, capability for altering work function, and cost-effectiveness in production when compared to alternative materials, rendering particularly well-suited for flexible, transparent MXene-based electrodes for various aesthetic solar window or rooftop panels and optoelectric devices.

(16) Research focus and exploration must also be made on non-Ti MXenes such as V, Nb, Mo, Cr-based carbides and nitrides. These can provide a prospect to understand the overall transparent MXenes, especially on non-Ti-based MXenes.

Acknowledgements

This work was supported by the Hong Kong Research Grants Council project (No. CityU 11201522).

Declaration of conflicting interests

The authors declare no conflicting interests regarding the content of this article.

Data availability

All data needed to support the conclusions in the paper are presented in the manuscript and/or the Supplementary Materials. Additional data related to this paper may be requested from the corresponding author upon request.

References

[1] Anasori, B.; Lukatskaya, M. R.; Gogotsi, Y. 2D metal carbides and nitrides (MXenes) for energy storage. *Nat. Rev. Mater.* **2017**, *2*, 16098.

[2] Naguib, M.; Mochalin, V. N.; Barsoum, M. W.; Gogotsi, Y. 25th anniversary article: MXenes: A new family of two-dimensional materials. *Adv. Mater.* **2014**, *26*, 992–1005.

[3] Zhang, J. Z.; Uzun, S.; Seyedin, S.; Lynch, P. A.; Akuzum, B.; Wang, Z. Y.; Qin, S.; Alhabeb, M.; Shuck, C. E.; Lei, W. W. et al. Additive-free MXene liquid crystals and fibers. *ACS Cent. Sci.* **2020**, *6*, 254–265.

[4] Wei, Y.; Zhang, P.; Soomro, R. A.; Zhu, Q. Z.; Xu, B. Advances in the synthesis of 2D MXenes. *Adv. Mater.* **2021**, *33*, 2103148.

[5] Naguib, M.; Kurtoglu, M.; Presser, V.; Lu, J.; Niu, J. J.; Heon, M.; Hultman, L.; Gogotsi, Y.; Barsoum, M. W. Two-dimensional nanocrystals produced by exfoliation of Ti_3AlC_2. *Adv. Mater.* **2011**, *23*, 4248–4253.

[6] Sang, X. H.; Xie, Y.; Lin, M. W.; Alhabeb, M.; Van Aken, K. L.; Gogotsi, Y.; Kent, P. R. C.; Xiao, K.; Unocic, R. R. Atomic defects in monolayer titanium carbide ($Ti_3C_2T_x$) MXene. *ACS Nano* **2016**, *10*, 9193–9200.

[7] Zhang, X. F.; Javed, M. S.; Ali, S.; Ahmad, A.; Shah, S. S. A.; Hussain, I.; Choi, D.; Tighezza, A. M.; Tag-Eldin, E.; Xia, C. L. et al. Band engineering in $Ti_2N/Ti_3C_2T_x$-MXene interface to enhance the performance of aqueous NH_4^+-ion hybrid supercapacitors. *Nano Energy* **2023**, *120*, 109108.

[8] Ling, Z.; Ren, C. E.; Zhao, M. Q.; Yang, J.; Giammarco, J. M.; Qiu, J. S.; Barsoum, M. W.; Gogotsi, Y. Flexible and conductive MXene films and nanocomposites with high capacitance. *Proc. Natl. Acad. Sci. USA* **2014**, *111*, 16676–16681.

[9] Mohapatra, D.; Kang, H. J.; Lee, S.; Son, Y.; Ansari, M. Z.; Kang, Y.; Lee, J. W.; Kim, S. H. Ultrahigh sensitivity for thermographic human–machine interface via precious metals atomic layer deposition on V-MXene: Computational and experimental exploration. *Small* **2024**, *20*, 2402003.

[10] Mohapatra, D.; Shin, Y.; Ansari, M. Z.; Kim, Y. H.; Park, Y. J.; Cheon, T.; Kim, H.; Lee, J. W.; Kim, S. H. Process controlled ruthenium on 2D engineered V-MXene via atomic layer deposition for human healthcare monitoring. *Adv. Sci.* **2023**, *10*, 2206355.

[11] Qin, R. Z.; Nong, J.; Wang, K. Q.; Liu, Y. S.; Zhou, S. B.; Hu, M. J.; Zhao, H. B.; Shan, G. C. Recent advances in flexible pressure sensors based on MXene materials. *Adv. Mater.* **2024**, *36*, 2312761.

[12] Mohapatra, D.; Byun, J. E.; Ansari, M. Z.; Kim, H.; Cheon, T.; Jang, J.; Cho, Y. R.; Lee, J. W.; Kim, S. H. Layer engineered MXene empowered wearable pressure sensors for non-invasive vital human–machine interfacing healthcare monitoring. *Adv. Mater. Technol.* **2023**, *8*, 2301175.

[13] Naguib, M.; Come, J.; Dyatkin, B.; Presser, V.; Taberna, P. L.; Simon, P.; Barsoum, M. W.; Gogotsi, Y. MXene: A promising transition metal carbide anode for lithium-ion batteries. *Electrochem. Commun.* **2012**, *16*, 61–64.

[14] Björk, J.; Rosen, J. Functionalizing MXenes by tailoring surface terminations in different chemical environments. *Chem. Mater.* **2021**, *33*, 9108–9118.

[15] Neelamana, H. V.; Rekha, S. M.; Bhat, S. V. $Ti_3C_2T_x$ MXene: A new promising 2D material for optoelectronics. *Chem. Mater.* **2023**, *35*, 7386–7405.

[16] Liu, X. H.; Zhang, W. R.; Zhang, X.; Zhou, Z. G.; Wang, C. F.; Pan, Y. M.; Hu, B.; Liu, C. T.; Pan, C. F.; Shen, C. Y. Transparent ultrahigh-molecular-weight polyethylene/MXene films with efficient UV-absorption for thermal management. *Nat. Commun.* **2024**, *15*, 3076.

[17] Pan, X. L.; Shen, L. H.; Schenning, A. P. H. J.; Bastiaansen, C. W. M. Transparent, high-thermal-conductivity ultradrawn polyethylene/graphene nanocomposite films. *Adv. Mater.* **2019**, *31*, 1904348.

[18] Liu, Z. X.; Alshareef, H. N. MXenes for optoelectronic devices. *Adv. Electron. Mater.* **2021**, *7*, 2100295.

[19] Huang, K.; Li, Z. J.; Lin, J.; Han, G.; Huang, P. Two-dimensional transition metal carbides and nitrides (MXenes) for biomedical applications. *Chem. Soc. Rev.* **2018**, *47*, 5109–5124.

[20] Khazaei, M.; Ranjbar, A.; Arai, M.; Sasaki, T.; Yunoki, S. Electronic

properties and applications of MXenes: A theoretical review. *J. Mater. Chem. C* **2017**, *5*, 2488–2503.
[21] Naguib, M.; Gogotsi, Y. Synthesis of two-dimensional materials by selective extraction. *Acc. Chem. Res.* **2015**, *48*, 128–135.
[22] Okubo, M.; Sugahara, A.; Kajiyama, S.; Yamada, A. MXene as a charge storage host. *Acc. Chem. Res.* **2018**, *51*, 591–599.
[23] Wang, H.; Wu, Y.; Yuan, X. Z.; Zeng, G. M.; Zhou, J.; Wang, X.; Chew, J. W. Clay-inspired MXene-based electrochemical devices and photo-electrocatalyst: State-of-the-art progresses and challenges. *Adv. Mater.* **2018**, *30*, 1704561.
[24] Yan, J.; Wang, Q.; Wei, T.; Fan, Z. J. Recent advances in design and fabrication of electrochemical supercapacitors with high energy densities. *Adv. Energy Mater.* **2014**, *4*, 1300816.
[25] Yuksel, R.; Sarioba, Z.; Cirpan, A.; Hiralal, P.; Unalan, H. E. Transparent and flexible supercapacitors with single walled carbon nanotube thin film electrodes. *ACS Appl. Mater. Interfaces* **2014**, *6*, 15434–15439.
[26] Chen, F. H.; Wan, P. B.; Xu, H. J.; Sun, X. M. Flexible transparent supercapacitors based on hierarchical nanocomposite films. *ACS Appl. Mater. Interfaces* **2017**, *9*, 17865–17871.
[27] Lu, X. H.; Yu, M. H.; Wang, G. M.; Tong, Y. X.; Li, Y. Flexible solid-state supercapacitors: Design, fabrication and applications. *Energy Environ. Sci.* **2014**, *7*, 2160–2181.
[28] Thirumurugan, A.; Dhanabalan, S. S.; Shanavas, S.; Udayabhaskar, R.; Morel, M. J.; Dineshbabu, N.; Ravichandran, K.; Schmidt-Mende, L.; Ramadoss, A. Hybrid supercapacitors, formation, and new advances with different electrochemical electrodes based on layered double hydroxides (LDHs), metal-organic framework (MOF) materials, smart supercapacitors. In *Smart Supercapacitors: Undamentals, Structures, and Applications*. Hussain, C. M.; Ahamed, M. B., Eds.; Elsevier: Amsterdam, 2023; pp 199–226.
[29] Lee, J. G.; Lee, J. H.; An, S.; Kim, D. Y.; Kim, T. G.; Al-Deyab, S. S.; Yarin, A. L.; Yoon, S. S. Highly flexible, stretchable, wearable, patternable and transparent heaters on complex 3D surfaces formed from supersonically sprayed silver nanowires. *J. Mater. Chem. A* **2017**, *5*, 6677–6685.
[30] Zhang, Y.; Guo, J. N.; Xu, D.; Sun, Y.; Yan, F. One-pot synthesis and purification of ultralong silver nanowires for flexible transparent conductive electrodes. *ACS Appl. Mater. Interfaces* **2017**, *9*, 25465–25473.
[31] Vosgueritchian, M.; Lipomi, D. J.; Bao, Z. N. Highly conductive and transparent PEDOT: PSS films with a fluorosurfactant for stretchable and flexible transparent electrodes. *Adv. Funct. Mater.* **2012**, *22*, 421–428.
[32] Zhu, Y.; Sun, Z. Z.; Yan, Z.; Jin, Z.; Tour, J. M. Rational design of hybrid graphene films for high-performance transparent electrodes. *ACS Nano* **2011**, *5*, 6472–6479.
[33] Dubal, D. P.; Chodankar, N. R.; Kim, D. H.; Gomez-Romero, P. Towards flexible solid-state supercapacitors for smart and wearable electronics. *Chem. Soc. Rev.* **2018**, *47*, 2065–2129.
[34] Liang, X.; Long, G. H.; Fu, C. W.; Pang, M. J.; Xi, Y. L.; Li, J. Z.; Han, W.; Wei, G. D.; Ji, Y. High performance all-solid-state flexible supercapacitor for wearable storage device application. *Chem. Eng. J.* **2018**, *345*, 186–195.
[35] Yang, Y. R.; Zhu, T.; Shen, L. N.; Liu, Y. H.; Zhang, D.; Zheng, B. W.; Gong, K.; Zheng, J.; Gong, X. Recent progress in the all-solid-state flexible supercapacitors. *SmartMat* **2022**, *3*, 349–383.
[36] Yu, M. H.; Feng, X. L. Thin-film electrode-based supercapacitors. *Joule* **2019**, *3*, 338–360.
[37] Zhao, Z. F.; Wang, S.; Wan, F.; Tie, Z.; Niu, Z. Q. Scalable 3D self-assembly of MXene films for flexible sandwich and microsized supercapacitors. *Adv. Funct. Mater.* **2021**, *31*, 2101302.
[38] Zhao, Z. F.; Wang, X. J.; Yao, M. J.; Liu, L. L.; Niu, Z. Q.; Chen, J. Activated carbon felts with exfoliated graphene nanosheets for flexible all-solid-state supercapacitors. *Chin. Chem. Lett.* **2019**, *30*, 915–918.
[39] Chen, C.; Cao, J.; Wang, X. Y.; Lu, Q. Q.; Han, M. M.; Wang, Q. R.; Dai, H. T.; Niu, Z. Q.; Chen, J.; Xie, S. S. Highly stretchable integrated system for micro-supercapacitor with AC line filtering and UV detector. *Nano Energy* **2017**, *42*, 187–194.
[40] Qi, D. P.; Liu, Z. Y.; Liu, Y.; Leow, W. R.; Zhu, B. W.; Yang, H.; Yu, J. C.; Wang, W.; Wang, H.; Yin, S. Y. et al. Suspended wavy graphene microribbons for highly stretchable microsupercapacitors. *Adv. Mater.* **2015**, *27*, 5559–5566.
[41] Hussain, I.; Sahoo, S.; Mohapatra, D.; Ahmad, M.; Iqbal, S.; Javed, M. S.; Gu, S.; Qin, N.; Lamiel, C.; Zhang, K. L. Recent progress in trimetallic/ternary-metal oxides nanostructures: Misinterpretation/misconception of electrochemical data and devices. *Appl. Mater. Today* **2022**, *26*, 101297.
[42] Cai, G. F.; Darmawan, P.; Cui, M. Q.; Wang, J. X.; Chen, J. W.; Magdassi, S.; Lee, P. S. Highly stable transparent conductive silver grid/PEDOT: PSS electrodes for integrated bifunctional flexible electrochromic supercapacitors. *Adv. Energy Mater.* **2016**, *6*, 1501882.
[43] Hasan, M. M.; Hossain, M. M. Nanomaterials-patterned flexible electrodes for wearable health monitoring: A review. *J. Mater. Sci.* **2021**, *56*, 14900–14942.
[44] An, T.; Cheng, W. L. Recent progress in stretchable supercapacitors. *J. Mater. Chem. A* **2018**, *6*, 15478–15494.
[45] De, S.; Lyons, P. E.; Sorel, S.; Doherty, E. M.; King, P. J.; Blau, W. J.; Nirmalraj, P. N.; Boland, J. J.; Scardaci, V.; Joimel, J. et al. Transparent, flexible, and highly conductive thin films based on polymer-nanotube composites. *ACS Nano* **2009**, *3*, 714–720.
[46] King, P. J.; Higgins, T. M.; De, S.; Nicoloso, N.; Coleman, J. N. Percolation effects in supercapacitors with thin, transparent carbon nanotube electrodes. *ACS Nano* **2012**, *6*, 1732–1741.
[47] Qi, D. P.; Liu, Y.; Liu, Z. Y.; Zhang, L.; Chen, X. D. Design of architectures and materials in in-plane micro-supercapacitors: Current status and future challenges. *Adv. Mater.* **2017**, *29*, 1602802.
[48] Amara, U.; Hussain, I.; Ahmad, M.; Mahmood, K.; Zhang, K. L. 2D MXene-based biosensing: A review. *Small* **2022**, 2205249.
[49] Du, Z. G.; Wu, C.; Chen, Y. C.; Cao, Z. J.; Hu, R. M.; Zhang, Y. Z.; Gu, J. N.; Cui, Y. L. S.; Chen, H.; Shi, Y. Z. et al. High-entropy atomic layers of transition-metal carbides (MXenes). *Adv. Mater.* **2021**, *33*, 2101473.
[50] Li, T. F.; Yao, L. L.; Liu, Q. L.; Gu, J. J.; Luo, R. C.; Li, J. H.; Yan, X. D.; Wang, W. Q.; Liu, P.; Chen, B. et al. Fluorine-free synthesis of high-purity $Ti_3C_2T_x$ (T = OH, O) via alkali treatment. *Angew. Chem., Int. Ed.* **2018**, *57*, 6115–6119.
[51] Natu, V.; Sokol, M.; Verger, L.; Barsoum, M. W. Effect of edge charges on stability and aggregation of $Ti_3C_2T_z$ MXene colloidal suspensions. *J. Phys. Chem. C* **2018**, *122*, 27745–27753.
[52] Shuck, C. E.; Han, M. K.; Maleski, K.; Hantanasirisakul, K.; Kim, S. J.; Choi, J.; Reil, W. E. B.; Gogotsi, Y. Effect of Ti_3AlC_2 MAX phase on structure and properties of resultant $Ti_3C_2T_x$ MXene. *ACS Appl. Nano Mater.* **2019**, *2*, 3368–3376.
[53] Lukatskaya, M. R.; Kota, S.; Lin, Z. F.; Zhao, M. Q.; Shpigel, N.; Levi, M. D.; Halim, J.; Taberna, P. L.; Barsoum, M. W.; Simon, P. et al. Ultra-high-rate pseudocapacitive energy storage in two-dimensional transition metal carbides. *Nat. Energy* **2017**, *2*, 17105.
[54] Zhan, C.; Naguib, M.; Lukatskaya, M.; Kent, P. R. C.; Gogotsi, Y.; Jiang, D. E. Understanding the MXene pseudocapacitance. *J. Phys. Chem. Lett.* **2018**, *9*, 1223–1228.
[55] Halim, J.; Lukatskaya, M. R.; Cook, K. M.; Lu, J.; Smith, C. R.; Näslund, L. Å.; May, S. J.; Hultman, L.; Gogotsi, Y.; Eklund, P. et al. Transparent conductive two-dimensional titanium carbide epitaxial thin films. *Chem. Mater.* **2014**, *26*, 2374–2381.
[56] Ren, S.; Pan, X. Y.; Zhang, Y. Y.; Xu, J. L.; Liu, Z. F.; Zhang, X. Y.; Li, X.; Gao, X.; Zhong, Y. N.; Chen, S. et al. Conductive MXene/polymer composites for transparent flexible supercapacitors. *Small* **2024**, *20*, 2401346.
[57] Guo, T. Z.; Zhou, D.; Deng, S. G.; Jafarpour, M.; Avaro, J.; Neels, A.; Heier, J.; Zhang, C. F. Rational design of $Ti_3C_2T_x$ MXene inks for conductive, transparent films. *ACS Nano* **2023**, *17*, 3737–3749.
[58] Nguyen, T. T.; Murali, G.; Nissimagoudar, A. S.; Bhatnagar, P.; Lee, S.; Patel, M.; Lee, S. C.; In, I.; Wong, C. P.; Kim, J. Flexible and

transparent MXene-platformed ultrafast photodetector for encrypted signal communication in self-powered operation. *Nano Energy* **2023**, *109*, 108331.
[59] Jung, M. Y.; Lee, C.; Park, J.; Son, J. W.; Yun, Y. J.; Jun, Y. Transparent supercapacitors with networked MXene on NiCo-layered double hydroxide. *Chem. Eng. J.* **2024**, *490*, 151556.
[60] Yuan, Y. J.; Jiang, L.; Li, X.; Zuo, P.; Zhang, X. Q.; Lian, Y. L.; Ma, Y. L.; Liang, M. S.; Zhao, Y.; Qu, L. T. Ultrafast shaped laser induced synthesis of MXene quantum dots/graphene for transparent supercapacitors. *Adv. Mater.* **2022**, *34*, 2110013.
[61] Couly, C.; Alhabeb, M.; Van Aken, K. L.; Kurra, N.; Gomes, L.; Navarro-Suárez, A. M.; Anasori, B.; Alshareef, H. N.; Gogotsi, Y. Asymmetric flexible MXene-reduced graphene oxide micro-supercapacitor. *Adv. Electron. Mater.* **2018**, *4*, 1700339.
[62] Zhang, C. F.; Anasori, B.; Seral-Ascaso, A.; Park, S. H.; McEvoy, N.; Shmeliov, A.; Duesberg, G. S.; Coleman, J. N.; Gogotsi, Y.; Nicolosi, V. Transparent, flexible, and conductive 2D titanium carbide (MXene) films with high volumetric capacitance. *Adv. Mater.* **2017**, *29*, 1702678.
[63] Wen, D.; Wang, X.; Liu, L.; Hu, C.; Sun, C.; Wu, Y. R.; Zhao, Y. L.; Zhang, J. X.; Liu, X. D.; Ying, G. B. Inkjet printing transparent and conductive MXene ($Ti_3C_2T_x$) films: A strategy for flexible energy storage devices. *ACS Appl. Mater. Interfaces* **2021**, *13*, 17766–17780.
[64] Singh, S. B.; Kshetri, T.; Singh, T. I.; Kim, N. H.; Lee, J. H. Embedded PEDOT: PSS/AgNFs network flexible transparent electrode for solid-state supercapacitor. *Chem. Eng. J.* **2019**, *359*, 197–207.
[65] Huang, L. S.; Lin, Y.; Zeng, W.; Xu, C.; Chen, Z. L.; Wang, Q.; Zhou, H. W.; Yu, Q. T.; Zhao, B. T.; Ruan, L. M. et al. Highly transparent and flexible Zn-$Ti_3C_2T_x$ MXene hybrid capacitors. *Langmuir* **2022**, *38*, 5968–5976.
[66] Wang, L. B.; Hu, X. L. Transparent electrodes for energy storage devices. *Batter. Supercaps* **2020**, *3*, 1275–1286.
[67] Zhang, C. F.; Nicolosi, V. MXenes for transparent conductive electrodes and transparent energy storage devices. In *2D Metal Carbides and Nitrides* (*MXenes*). Anasori, B.; Gogotsi, Y., Eds.; Springer: Cham, 2019; pp 481–501.
[68] Ebrahimi, M.; Mei, C. T. Optoelectronic properties of $Ti_3C_2T_x$ MXene transparent conductive electrodes: Microwave synthesis of parent MAX phase. *Ceram. Int.* **2020**, *46*, 28114–28119.
[69] Ying, G. B.; Kota, S.; Dillon, A. D.; Fafarman, A. T.; Barsoum, M. W. Conductive transparent V_2CT_x (MXene) films. *FlatChem* **2018**, *8*, 25–30.
[70] Lee, S.; Kim, E. H.; Yu, S.; Kim, H.; Park, C.; Lee, S. W.; Han, H.; Jin, W.; Lee, K.; Lee, C. E. et al. Polymer-laminated $Ti_3C_2T_x$ MXene electrodes for transparent and flexible field-driven electronics. *ACS Nano* **2021**, *15*, 8940–8952.
[71] Liu, J.; Zhang, L.; Wang, N.; Li, C. Z. Highly stretchable and transparent triboelectric nanogenerator based on multilayer structured stable electrode for self-powered wearable sensor. *Nano Energy* **2020**, *78*, 105385.
[72] Tang, H. H.; Feng, H. R.; Wang, H. K.; Wan, X. J.; Liang, J. J.; Chen, Y. S. Highly conducting MXene-silver nanowire transparent electrodes for flexible organic solar cells. *ACS Appl. Mater. Interfaces* **2019**, *11*, 25330–25337.
[73] Kumar, S.; Kang, D.; Nguyen, V. H.; Nasir, N.; Hong, H.; Kim, M.; Nguyen, D. C.; Lee, Y. J.; Lee, N.; Seo, Y. Application of titanium-carbide MXene-based transparent conducting electrodes in flexible smart windows. *ACS Appl. Mater. Interfaces* **2021**, *13*, 40976–40985.
[74] Ahn, S.; Han, T. H.; Maleski, K.; Song, J.; Kim, Y. H.; Park, M. H.; Zhou, H. Y.; Yoo, S.; Gogotsi, Y.; Lee, T. W. A 2D titanium carbide MXene flexible electrode for high-efficiency light-emitting diodes. *Adv. Mater.* **2020**, *32*, 2000919.
[75] Jiang, W.; Lee, S.; Zhao, K. Y.; Lee, K.; Han, H.; Oh, J.; Lee, H.; Kim, H.; Koo, C. M.; Park, C. Flexible and transparent electrode of hybrid $Ti_3C_2T_x$ MXene-silver nanowires for high-performance quantum dot light-emitting diodes. *ACS Nano* **2022**, *16*, 9203–9213.
[76] Chen, J. X.; Li, Z. L.; Ni, F. L.; Ouyang, W. X.; Fang, X. S. Bio-inspired transparent MXene electrodes for flexible UV photodetectors. *Mater. Horiz.* **2020**, *7*, 1828–1833.

Iftikhar Hussain is a Researcher at the City University of Hong Kong. He received his M.S. degree from Yeungnam University, South Korea and Ph.D. degree from City University of Hong Kong under the supervision of Prof. Kaili Zhang. He also worked as a visiting researcher at Drexel University, USA, under the supervision of Prof. Yury Gogotsi. His current research focuses on the development of electrode materials for energy storage/conversions. He has published his research/review articles in refereed journals such as *Prog. Mater. Sci., PECS, Adv. Mater., Adv. Energy Mater., Mater. Sci. Eng. R Rep., Adv. Funct. Mater., Adv. Sci., ACS Energy Lett., Mater. Today, Coord. Chem. Rev., Energy Storage Mater., Small, Carbon Energy, Nanomicro Lett., Nano Energy, J. Mater. Chem. A, ACS Appl. Mater. Interfaces., J. Energy Chem., Chem. Eng. J, Adv. Colloid Interface Sci., J. Power Sources*, etc.

Kaili Zhang is a Professor in the Department of Mechanical Engineering at City University of Hong Kong. He received his Ph.D. degree from the National University of Singapore in 2006. He then worked as a postdoctoral researcher at French National Center for Scientific Research (LAASCNRS) and Swiss Federal Institute of Technology Zurich (ETH Zurich). He joined the City University of Hong Kong as an assistant professor in 2009. His research interests include nanomaterials for energy storage/conversions, energetic materials, and energetics-on-a-chip. He has published more than 200 peer-reviewed papers/reviews in reputed journals.